Crystallographic and magnetic properties of the hydrides $R_3Fe_{29-x}Cr_xH_y$ (R = Y, Ce, Nd, Sm, Gd, Tb, and Dy)

1998 J. Phys.: Condens. Matter 10 7037

(http://iopscience.iop.org/0953-8984/10/31/019)

J. Phys.: Condens. Matter **10** (1998) 7037–7047. Printed in the UK PII: S0953-8984(98)92724-2

Crystallographic and magnetic properties of the hydrides $R_3Fe_{29-x}Cr_xH_y$ (R = Y, Ce, Nd, Sm, Gd, Tb, and Dy)

Xiu-Feng Han†‡, Ren-Geng Xu§, Xin-Hua Wang§, H G Pan§, T Miyazaki‖, E Baggio-Saitovitch¶, F M Yang‡ and C P Cheng§

† Material Science Centre, Institute of Semiconductors, Chinese Academy of Sciences, PO Box 912, Beijing 100083, People's Republic of China

‡ Institute of Physics, Chinese Academy of Sciences, PO Box 603, Beijing 100080, People's Republic of China

§ Materials Department of Zhejiang University, Hangzhou 310027, People's Republic of China

‖ Department of Applied Physics, Faculty of Engineering, Tohoku University, Sendai 980-77, Japan

¶ Centro Brasileiro de Pesquisas Físicas, Rua Dr Xavier Sigaud, No 150-Urac-RJ, Brazil

Received 23 March 1998, in final form 18 May 1998

Abstract. A systematic study of the structural and intrinsic magnetic properties of the hydrides $R_3Fe_{29-x}Cr_xH_y$ (R = Y, Ce, Nd, Sm, Gd, Tb, and Dy) has been performed. Hydrogenation leads to a relative volume expansion of the unit cell and a decrease in x-ray density for each compound. Anisotropic expansions mainly along the *a*- and *b*-axes rather than along the *c*-axis for all of the compounds upon hydrogenation are observed. The lattice constants and the unit-cell volume of $R_3Fe_{29-x}Cr_x$ and $R_3Fe_{29-x}Cr_xH_y$ decrease with increasing R atomic number from Nd to Dy, except for Ce, reflecting the lanthanide contraction. Hydrogenation results in an increase in the Curie temperature and a corresponding increase in the saturation magnetization at room temperature for each compound. After hydrogenation a decrease of 0.34 μ_B/Fe in the average Fe atomic magnetic moment and a slight increase in the anisotropy field for $Y_3Fe_{27.2}Cr_{1.8}$ are achieved at 4.2 K. First-order magnetization processes (FOMP) occur in magnetic fields of around 1.5 T and 4.0 T at 4.2 K for $Nd_3Fe_{24.5}Cr_{4.5}H_{5.0}$ and $Tb_3Fe_{27.0}Cr_{2.0}H_{2.8}$, and around 1.4 T at room temperature for $Gd_3Fe_{28.0}Cr_{1.0}H_{4.2}$. The abnormal crystallographic and magnetic properties of $Ce_3Fe_{25.0}Cr_{4.0}$ and $Ce_3Fe_{25.0}Cr_{4.0}H_{5.4}$ suggest that the Ce ion is non-triply ionized.

1. Introduction

A new class of rare-earth–iron (R–Fe) compounds stabilized by a third element (T = transition metal), located at the iron-rich corner in the R–Fe–T phase diagrams, have been synthesized [1, 2]. This class was recognized as having the $Nd_3(Fe, Ti)_{29}$ stoichiometry with monoclinic symmetry [3] and the $A2/m$ space group [4] by x-ray powder diffraction (XRD), and then this was confirmed by neutron powder diffraction [5, 6]. Subsequent work on its interstitial nitrides and carbides indicated that the $Sm_3(Fe, Ti)_{29}N_y$ [7–9] compounds can be regarded as new candidates for hard-magnet application, which further aroused interest in intensive investigations of the structural and magnetic properties of $R_3(Fe, T)_{29}$ compounds.

Many members in this series of $R_3(Fe, T)_{29}$ compounds, such as $R_3(Fe, Ti)_{29}$ (R = Ce, Pr, Nd, Sm, [10–12] Gd [13, 14], Tb [15], and Y [16, 17]), $R_3(Fe, V)_{29}$ (R = Sm [18–20], Y, Nd, Gd [18, 20], Ce, Tb, and Dy [20–22]), $R_3(Fe, Cr)_{29}$ (R = Ce, Nd, [10, 20, 23],

0953-8984/98/317037+11$19.50

Sm [10, 19, 20, 24], Gd, Tb, Dy, and Y [20, 25]), $Nd_3(Fe, Mn)_{29}$ [26], and $R_3(Fe, Mo)_{29}$ (R = Ce, Nd, Sm, Gd, Tb, Dy, and Y) [27], have been formed with a good single-phase quality. The crystallographic structure, the intrinsic magnetic properties, the neutron powder diffraction, the ^{57}Fe Mössbauer spectra, and the hyperfine fields of these compounds have been studied in detail by the authors and by other researchers [4, 5, 6, 28].

Simultaneously, in order to develop new hard magnets, many experimental studies on their interstitial nitrides and carbides have been reported. The nitrides $Sm_3(Fe, T)_{29}N_y$ (T = Ti [7, 8, 29], V [19, 30], Cr [19, 24, 31, 32], and Mo [27]) and the carbides $Sm_3(Fe, T)_{29}C_y$ (T = Ti [9, 29] and Cr [33]) were considered as potential candidates for permanent-magnet applications.

Up to now, little investigation has been carried out on their interstitial hydrides. Only studies of $Nd_3(Fe, Ti)_{29}H_y$ [11] and $Sm_3(Fe, T)_{29}H_y$ (T = Ti, V, and Cr) [19] have been reported. It is well known that metal hydrides are interesting candidates for applications in the areas of thermal storage media, heat pumps, and cooling systems [34]. In order to understand this novel class of R–Fe compounds and to develop new metal hydride materials, further study on the structure and magnetic properties of the hydrides of these 3:29 compounds is necessary.

In this work, experimental information on the syntheses, lattice parameters, and intrinsic magnetic properties of hydrides formed by the absorption of hydrogen gas in the compounds $R_3Fe_{29-x}Cr_xH_y$ (R = Y, Ce, Nd, Sm, Gd, Tb, and Dy) has been obtained.

2. Experimental methods

Ingots with composition $R_3Fe_{29-x}Cr_x$ (R = Y, Ce, Nd, Sm, Gd, Tb, and Dy) were prepared by argon arc melting the constituent elements, with purities of at least 99.9%. The starting composition contained 5–10% excess of rare-earth elements compared with the stoichiometric composition $R_3Fe_{29-x}Cr_x$, to compensate for the loss of the rare earth during melting and annealing. Then the ingots were sealed in quartz tubes filled with an argon atmosphere and annealed at 1183–1323 K for a period of from one day to five days in order to maximize the amount of $R_3Fe_{29-x}Cr_x$ phase; this was followed by quenching in water. The 3:29 single-phase character of the ingots was examined by both x-ray diffraction (XRD) with Cu Kα radiation and thermomagnetic analysis (TMA).

To prepare the hydrides, the single-phase 3:29 ingots were pulverized into fine powders with an average size of 100–1000 μm. Hydrogenation was performed by heating the fine particles in hydrogen at 5 atm and at 573 K for R = Ce, Nd, Sm, Gd, and Tb or at 673 K for R = Y and Dy for a period of 2–4 hours in a high-pressure container. The XRD patterns and TMA showed that all of the hydrides of $R_3Fe_{29-x}Cr_x$ crystallized in the $Nd_3(Fe, Ti)_{29}$-type structure, except a small amount of α-Fe in some samples. The hydrogen concentration in each hydride $R_3Fe_{29-x}Cr_xH_y$ was deduced from the difference between the pressure before hydrogenation and that after according to the gas-state equation $PV = nRT$ at a constant temperature.

TMA was performed in a low field of 0.04 T with a vibrating-sample magnetometer (VSM) from room temperature (RT) to above the Curie temperature. XRD with Cu Kα radiation was used to determine the lattice parameters. In order to obtain the saturation magnetization and anisotropy field at 4.2 K and RT for the magnetically aligned samples of $R_3Fe_{29-x}Cr_xH_y$, the VSM was used to measure the magnetic isotherms at 4.2 K, and the pulsed magnetic fields (PMF) up to 12 T, together with the singular-point detection (SPD) technique [35], were utilized to obtain the magnetic isotherms and the SPD signal plots (dM^2/dt^2 versus H) at RT. According to the SPD theory [35], a singularity in the second

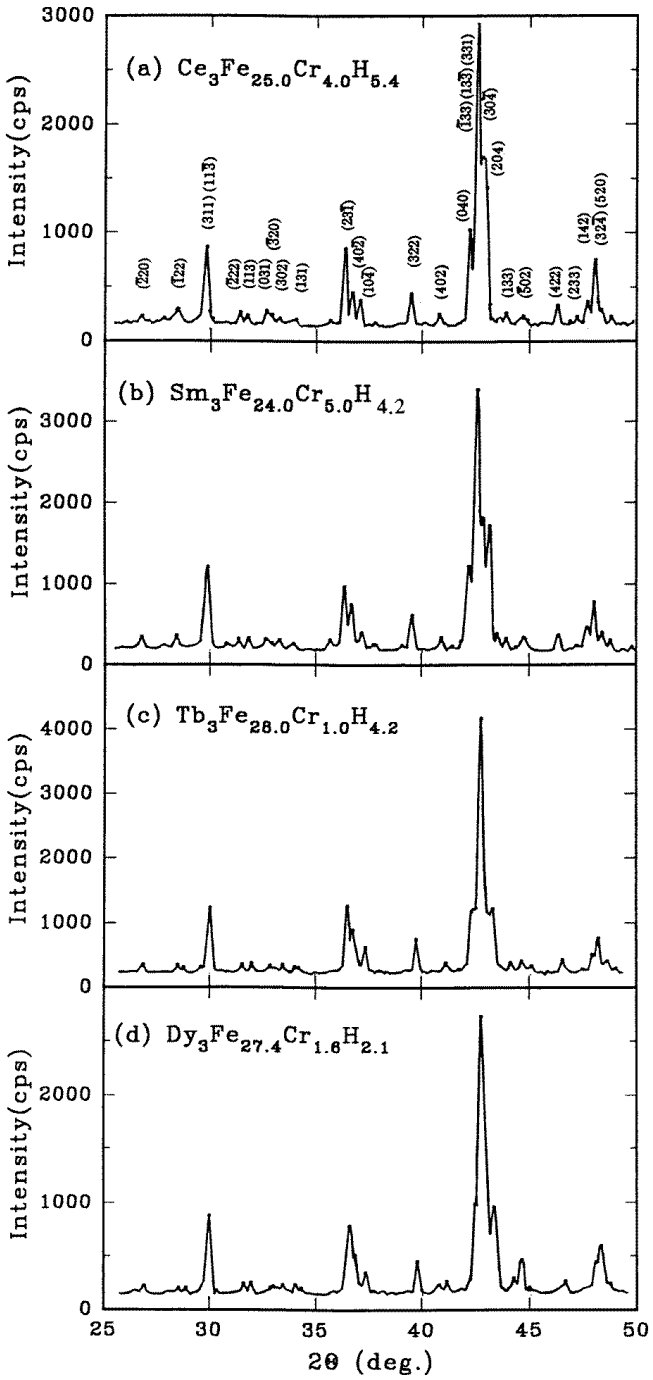

Figure 1. XRD patterns with Cu Kα radiation for $R_3Fe_{29-x}Cr_xH_y$ (R = Ce (a), Sm (b), Tb (c), and Dy (d)).

derivative of the magnetization M with respect to the magnetic field H can be observed at the anisotropy field H_A. Similarly, this method can also be used to detect a first-order magnetization process (FOMP). The preparation and measuring procedure for magnetically aligned samples was described in our previous studies [20, 25].

3. Results and discussion

3.1. Crystallographic properties

Figure 1 shows XRD patterns obtained with Cu Kα radiation for $R_3Fe_{29-x}Cr_xH_y$ (R = Ce, Sm, Tb, and Dy). The patterns can be indexed well assuming the $Nd_3(Fe, Ti)_{29}$-type structure with monoclinic symmetry and the $A2/m$ space group. As an example, the indices (h, k, l) of $Ce_3Fe_{25.0}Cr_{4.0}H_{5.4}$ are given in figure 1(a). The peak positions of the XRD for each hydride are shifted to lower angles compared to those for $R_3Fe_{29-x}Cr_x$ (R = Y, Ce, Nd, Sm, Gd, Tb, and Dy) [20] which demonstrates the increase of the lattice parameters after hydrogenation.

Table 1 gives the crystallographic parameters, the unit-cell volume, and the density ρ derived on the basis of the analysis of XRD data for all of the hydrides investigated here, together with their parent compounds. The crystallographic parameters were obtained by fitting the XRD patterns with monoclinic symmetry and the $A2/m$ space group. After hydrogenation, the average relative volume expansion is about 2%, except for Ce, Tb, and Dy for which the larger and smaller amounts of the absorbed interstitial H atoms in their compounds resulted in larger and smaller expansions of their unit-cell volumes. Hydrogenation leads to a decrease in x-ray density for each compound owing to its relative volume expansion.

Like for the parent compounds $R_3Fe_{29-x}Cr_x$, it can been seen that the lattice constants and the unit-cell volume of $R_3Fe_{29-x}Cr_xH_y$ decrease with increasing R atomic number

Table 1. The lattice parameters, a, b, c, β, and the unit-cell volume $V = abc\sin\beta$ derived on the basis of the analysis of x-ray data with the $A2/m$ space group, and the x-ray density ρ derived from the lattice constants for $R_3Fe_{29-x}Cr_x$ and $R_3Fe_{29-x}Cr_xH_y$ (R = Y, Ce, Nd, Sm, Gd, Tb, and Dy) compounds.

$R_3Fe_{29-x}Cr_x(H_y)$	a (nm)	b (nm)	c (nm)	β (deg)	V (nm^3)	ρ (g cm^{-3})
$Y_3Fe_{27.2}Cr_{1.8}$	1.0570	0.8474	0.9653	96.98	0.8582	7.273
$Ce_3Fe_{25.0}Cr_{4.0}$	1.0527	0.8484	0.9668	96.67	0.8576	7.771
$Nd_3Fe_{24.5}Cr_{4.5}$	1.0615	0.8556	0.9714	96.90	0.8759	7.685
$Sm_3Fe_{24.0}Cr_{5.0}$	1.0585	0.8521	0.9684	96.90	0.8671	7.857
$Gd_3Fe_{28.0}Cr_{1.0}$	1.0604	0.8515	0.9686	96.95	0.8682	7.985
$Tb_3Fe_{28.0}Cr_{1.0}$	1.0585	0.8492	0.9675	96.92	0.8634	8.049
$Tb_3Fe_{27.0}Cr_{2.0}$	1.0559	0.8494	0.9666	96.89	0.8607	8.059
$Dy_3Fe_{27.4}Cr_{1.6}$	1.0556	0.8475	0.9655	96.91	0.8574	8.138
$Y_3Fe_{27.2}Cr_{1.8}H_{3.8}$	1.0625	0.8528	0.9686	97.18	0.8708	7.183
$Ce_3Fe_{25.0}Cr_{4.0}H_{5.4}$	1.0640	0.8563	0.9731	96.87	0.8800	7.593
$Nd_3Fe_{24.5}Cr_{4.5}H_{5.0}$	1.0714	0.8620	0.9770	97.07	0.8955	7.559
$Sm_3Fe_{24.0}Cr_{5.0}H_{4.2}$	1.0658	0.8582	0.9721	97.11	0.8823	7.730
$Gd_3Fe_{28.0}Cr_{1.0}H_{4.2}$	1.0664	0.8580	0.9724	97.17	0.8828	7.869
$Tb_3Fe_{28.0}Cr_{1.0}H_{4.2}$	1.0647	0.8558	0.9712	97.20	0.8780	7.931
$Tb_3Fe_{27.0}Cr_{2.0}H_{2.8}$	1.0614	0.8537	0.9676	97.15	0.8700	7.984
$Dy_3Fe_{27.4}Cr_{1.6}H_{2.1}$	1.0593	0.8508	0.9666	97.07	0.8646	8.078

Table 2. The expansions $\delta a/a$, $\delta b/b$, and $\delta c/c$ of the lattice parameters, and the expansion $\delta V/V$ of the unit-cell volume $V = abc\sin\beta$ derived on the basis of the analysis of x-ray data with the $A2/m$ space group, and the variations $\delta\beta/\beta$ and $\delta\rho/\rho$ of the angle β and the x-ray density ρ derived from the lattice constants for $R_3Fe_{29-x}Cr_xH_y$ (R = Y, Ce, Nd, Sm, Gd, Tb, and Dy) hydrides compared with the values for their parent compounds.

$R_3Fe_{29-x}Cr_xH_y$	$\delta a/a$ (%)	$\delta b/b$ (%)	$\delta c/c$ (%)	$\delta\beta/\beta$ (%)	$\delta V/V$ (%)	$\delta\rho/\rho$ (%)
$Y_3Fe_{27.2}Cr_{1.8}H_{3.8}$	0.52	0.63	0.34	0.21	1.5	−1.2
$Ce_3Fe_{25.0}Cr_{4.0}H_{5.4}$	1.07	0.93	0.65	0.21	2.6	−2.3
$Nd_3Fe_{24.5}Cr_{4.5}H_{5.0}$	0.93	0.75	0.58	0.18	2.2	−1.6
$Sm_3Fe_{24.0}Cr_{5.0}H_{4.2}$	0.69	0.72	0.38	0.22	1.8	−1.6
$Gd_3Fe_{28.0}Cr_{1.0}H_{4.2}$	0.57	0.76	0.39	0.23	1.7	−1.4
$Tb_3Fe_{28.0}Cr_{1.0}H_{4.2}$	0.59	0.78	0.38	0.29	1.7	−1.5
$Tb_3Fe_{27.0}Cr_{2.0}H_{2.8}$	0.52	0.51	0.10	0.27	1.1	−0.93
$Dy_3Fe_{27.4}Cr_{1.6}H_{2.1}$	0.35	0.39	0.11	0.17	0.84	−0.74

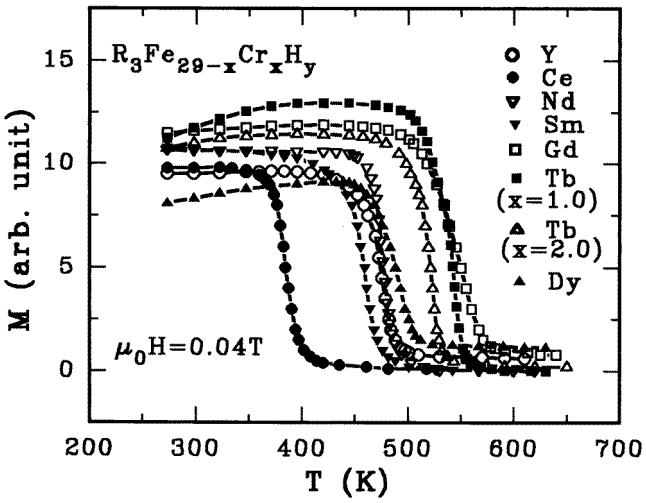

Figure 2. Thermomagnetic curves for $R_3Fe_{29-x}Cr_xH_y$ (R = Y, Ce, Nd, Sm, Gd, Tb, and Dy) in a low field of 0.04 T.

from Nd to Dy, except for Ce, reflecting the lanthanide contraction. The decrease of the unit-cell volume results in an increase in density with increasing R atomic number from Nd to Dy, except for Ce. The lattice constants and unit-cell volume of $Ce_3Fe_{25.0}Cr_{4.0}$ and $Ce_3Fe_{25.0}Cr_{4.0}H_{5.4}$ are unusually smaller than those of $R_3Fe_{29-x}Cr_x$ and $R_3Fe_{29-x}Cr_xH_y$ (R = Nd and Sm). These abnormal properties maybe associated with the Ce ion being non-triply ionized in each series of $R_3Fe_{29-x}Cr_x$ and $R_3Fe_{29-x}Cr_xH_y$ compounds. A larger fraction of the interstitial hydrogen atoms in the $Ce_3Fe_{25.0}Cr_{4.0}H_{5.4}$ resulted in an expansion of the lattice constant c, which was slightly larger than that of $R_3Fe_{29-x}Cr_xH_y$ (R = Nd and Sm).

Table 2 gives the expansions of the lattice parameters and the unit-cell volume, and the variations of the angle β and the x-ray density ρ upon hydrogenation for each hydride compared with the value for its parent compound. It can be seen that the lattice expansions are different along the a-, b-, and c-axis for each hydride in this series of compounds. The

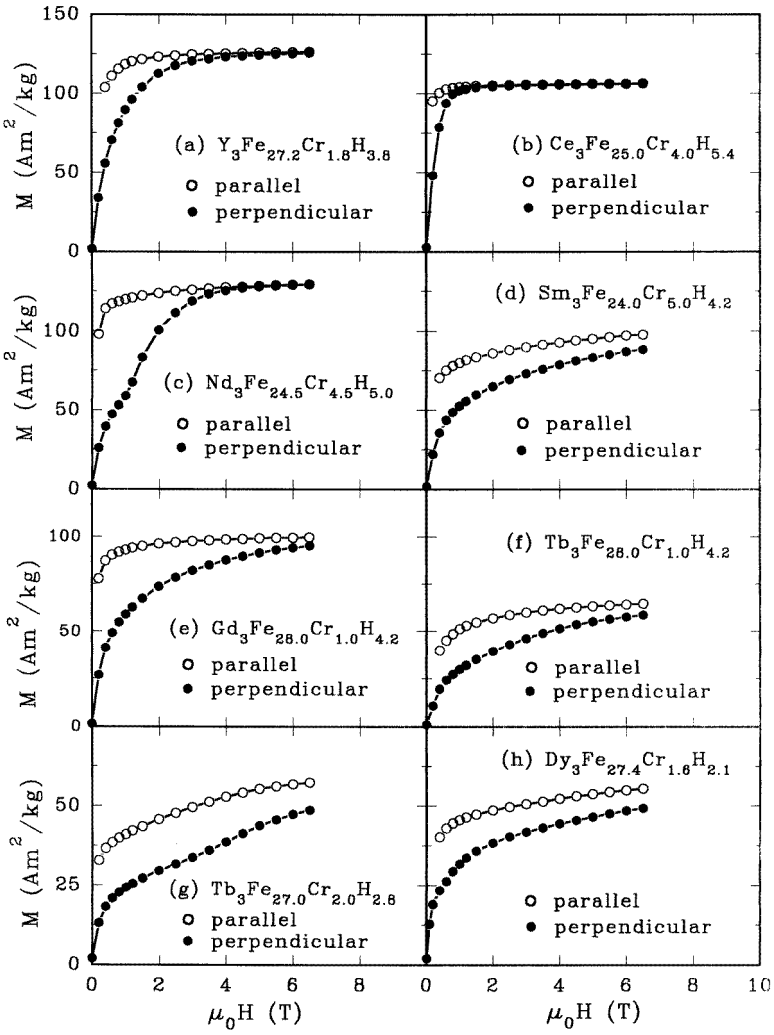

Figure 3. Magnetic isotherms at 4.2 K for $R_3Fe_{29-x}Cr_xH_y$ (R = Y, Ce, Nd, Sm, Gd, Tb, and Dy) measured with a VSM in an external field applied either parallel or perpendicular to the alignment direction of the powder samples.

anisotropic expansions of $R_3Fe_{29-x}Cr_xH_y$, such as

$$\frac{\delta a}{a} \simeq \frac{\delta b}{b} > \frac{\delta c}{c}$$

for R = Y, Ce, Nd, Sm, Gd, Tb and Dy, indicate that the expansions occur mainly in the basal *c*-plane rather than along the *c*-axis for all of the hydrides. These results are in agreement with the hypothesis that hydrogen atoms mainly occupy the 4i and 4f sites with the $A2/m$ space group (corresponding to the $4e_1$ and $4e_2$ sites with the $P21/c$ space group [19, 5]) which are located in the basal plane referred to the 1:5 cell [19].

3.2. Magnetic properties

Figure 2 shows thermomagnetic curves of $R_3Fe_{29-x}Cr_xH_y$ (R = Y, Ce, Nd, Sm, Gd, Tb, and Dy) measured in a low field of 0.04 T on free-powder samples and by using a VSM from RT to above the Curie temperature. The Curie temperature T_C was deduced from M^2–T plots, derived from the thermomagnetic curve $M(T)$, by extrapolating M to zero. Hydrogenation leads to an increase in the Curie temperature T_C of $R_3Fe_{29-x}Cr_x$. On average, the increase over the values for their parent compounds reaches about 70 K.

Figure 3 displays the magnetic isotherms at 4.2 K for the magnetically aligned samples of $R_3Fe_{29-x}Cr_xH_y$ (R = Y (a), Ce (b), Nd (c), Sm (d), Gd (e), Tb ((f), $x = 1.0$), Tb ((g), $x = 2.0$) and Dy (h)) measured with a VSM. A first-order magnetization process (FOMP) occurs in magnetic fields of around 1.5 T and 4.0 T at 4.2 K for $Nd_3Fe_{24.5}Cr_{4.5}H_{5.0}$ and $Tb_3Fe_{27.0}Cr_{2.0}H_{2.8}$, respectively.

Figure 4 illustrates the magnetic isotherms at RT for the magnetically aligned samples of $R_3Fe_{29-x}Cr_xH_y$ (R = Y (a), Ce (b), Nd (c), Sm (d), Gd (e), Tb ((f), $x = 1.0$), Tb ((g), $x = 2.0$) and Dy (h)) measured with a PMF up to 12 T, together with the SPD signal plots (d^2M/dt^2 versus H). Singularities, indicating the critical field H_{cr} at which the FOMP occurs or the anisotropy field H_A at which the saturation magnetization is achieved, are clearly detectable from the curves of d^2M/dt^2 versus H measured for the magnetically aligned samples. As an example, the singularities at around 1.4 T and 2.9 T in the curves of d^2M/dt^2 versus H at RT for $Gd_3Fe_{28.0}Cr_{1.0}H_{4.2}$ correspond to the critical field H_{cr} and the anisotropy field H_A.

Table 3. The saturation magnetization at 4.2 K and room temperature (RT) for $R_3Fe_{29-x}Cr_x$ and $R_3Fe_{29-x}Cr_xH_y$ (R = Y, Ce, Nd, Sm, Gd, Tb, and Dy) compounds.

$R_3Fe_{29-x}Cr_xH_y$	M_S(4.2 K) (A m^2 kg^{-1})	M_S(RT) (A m^2 kg^{-1})	$R_3Fe_{29-x}Cr_x$	M_S(4.2 K) (A m^2 kg^{-1})	M_S(RT) (A m^2 kg^{-1})
$Y_3Fe_{27.2}Cr_{1.8}H_{3.8}$	127.4	119.6	$Y_3Fe_{27.2}Cr_{1.8}$	155.0	114.7
$Ce_3Fe_{25.0}Cr_{4.0}H_{5.4}$	107.1	94.3	$Ce_3Fe_{25.0}Cr_{4.0}$	110.0	54.4
$Nd_3Fe_{24.5}Cr_{4.5}H_{5.0}$	103.9	111.7	$Nd_3Fe_{24.5}Cr_{4.5}$	137.0	88.3
$Sm_3Fe_{24.0}Cr_{5.0}H_{4.2}$	102.3	89.0	$Sm_3Fe_{24.0}Cr_{5.0}$	98.0	80.1
$Gd_3Fe_{28.0}Cr_{1.0}H_{4.2}$	100.3	112.4	$Gd_3Fe_{28.0}Cr_{1.0}$	96.0	87.7
$Tb_3Fe_{28.0}Cr_{1.0}H_{4.2}$	66.6	92.9	$Tb_3Fe_{28.0}Cr_{1.0}$	70.2	80.7
$Tb_3Fe_{27.0}Cr_{2.0}H_{2.8}$	60.4	88.0	$Tb_3Fe_{27.0}Cr_{2.0}$	57.0	58.7
$Dy_3Fe_{27.4}Cr_{1.6}H_{2.1}$	58.1	86.4	$Dy_3Fe_{27.4}Cr_{1.6}$	60.0	69.9

The saturation magnetization M_S of the hydrides $R_3Fe_{29-x}Cr_xH_y$ (R = Y, Ce, Nd, Sm, Gd, Tb, and Dy) and their parent compounds at 4.2 K and RT investigated here are listed in table 3. The values of the saturation magnetization at 4.2 K and at RT were derived from the high-field data of the magnetization curves measured in the external field applied parallel to the alignment direction of the powder samples, based on the law of approach to saturation.

Table 4 gives the Curie temperature T_C, the saturation magnetization M_S, and the anisotropy field H_A at 4.2 K and RT for the hydrides $R_3Fe_{29-x}Cr_xH_y$ (R = Y, Ce, Nd, Sm, Gd, Tb, and Dy) and their parent compounds. In this table, the units of the saturation magnetization at 4.2 K and at RT were converted from A m^2 kg^{-1} into μ_B/f.u. for use in the discussion of the physics. The anisotropy field H_A at 4.2 K was deduced from the intercept of the two magnetization curves, by extrapolating the straight-line parts, measured in magnetic fields applied parallel and perpendicular to the alignment direction of the powder

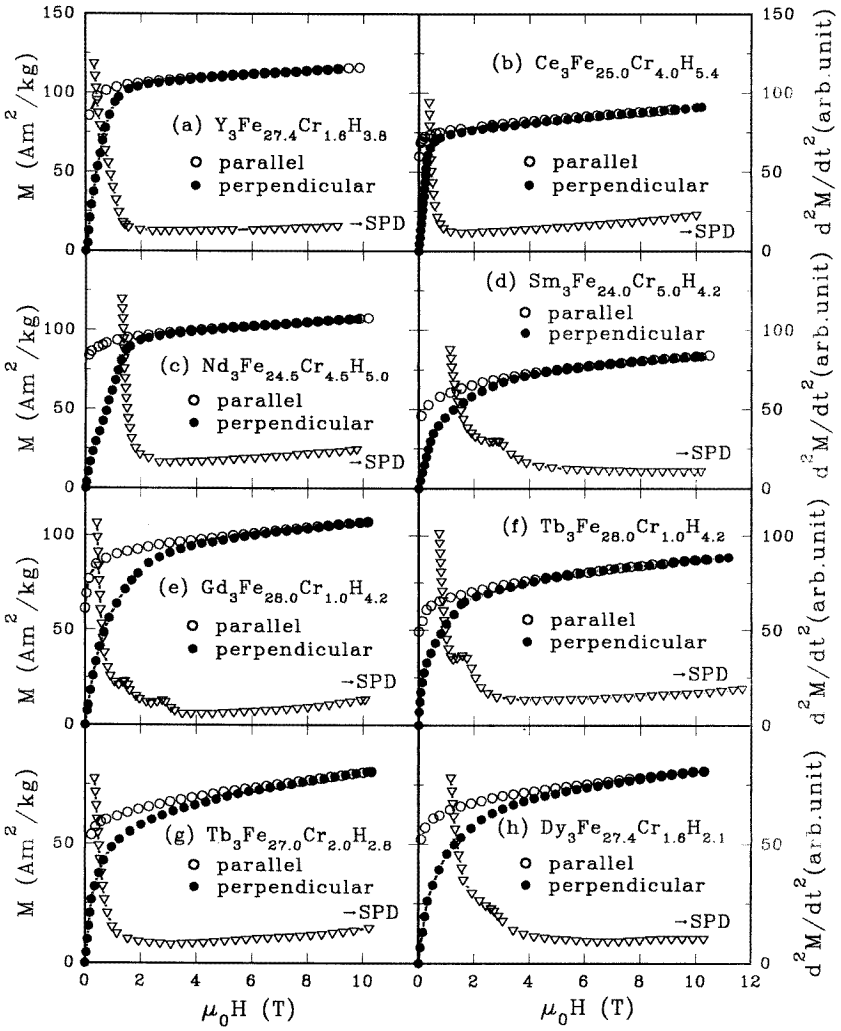

Figure 4. Magnetic isotherms and SPD signals at RT for $R_3Fe_{29-x}Cr_xH_y$ (R = Y, Ce, Nd, Sm, Gd, Tb, and Dy) measured with a PMF in an external field applied either parallel or perpendicular to the alignment direction of the powder samples.

samples. The anisotropy field H_A at RT was determined from the singularities in the SPD signal plots (dM^2/dt^2 versus H) or the intercept of the two magnetization curves measured in magnetic fields applied parallel and perpendicular to the alignment direction of the powder samples.

It can be seen that introducing H as interstitial atoms resulted in improvements for all of the hydrides $R_3Fe_{29-x}Cr_xH_y$ in the saturation magnetization at RT compared with those of their parent compounds owing to the increase in Curie temperature. Hydrogenation also led to an increase for $R_3Fe_{29-x}Cr_x$ with R = Sm, Gd, Tb ($x = 2.0$), and Dy, and a decrease for $R_3Fe_{29-x}Cr_x$ with R = Y, Ce, Nd, and Tb ($x = 1.0$) in the saturation magnetization at 4.2 K. After hydrogenation, an increase for $R_3Fe_{29-x}Cr_x$ with R = Y, Sm, and Tb ($x = 2.0$) and a decrease for $Dy_3Fe_{27.4}Cr_{1.6}$ in the anisotropy field both at 4.2 K and RT are observed.

Table 4. The Curie temperature T_C, the saturation magnetization M_S, and the anisotropy field H_A at 4.2 K and room temperature (RT) for $R_3Fe_{29-x}Cr_x$ and $R_3Fe_{29-x}Cr_xH_y$ (R = Y, Ce, Nd, Sm, Gd, Tb, and Dy) compounds.

$R_3Fe_{29-x}Cr_x(H_y)$	T_C (K)	M_S(4.2 K) (μ_B/f.u.)	M_S(RT) (μ_B/f.u.)	$\mu_0 H_A$(4.2 K) (T)	$\mu_0 H_A$(RT) (T)
$Y_3Fe_{27.2}Cr_{1.8}$	427	52.2	38.6	3.4	1.4
$Ce_3Fe_{25.0}Cr_{4.0}$	317	39.5	19.7	2.5	0.6
$Nd_3Fe_{24.5}Cr_{4.5}$	413	49.9	32.2	9.1	1.2
$Sm_3Fe_{24.0}Cr_{5.0}$	424	36.0	29.4	9.6	2.7
$Gd_3Fe_{28.0}Cr_{1.0}$	507	35.9	32.8	7.7	3.6
$Tb_3Fe_{28.0}Cr_{1.0}$	465	26.3	30.2	9.2	3.2
$Tb_3Fe_{27.0}Cr_{2.0}$	470	21.3	22.0	9.8	3.7
$Dy_3Fe_{27.4}Cr_{1.6}$	442	22.6	26.3	14.1	4.6
$Y_3Fe_{27.2}Cr_{1.8}H_{3.8}$	488	43.0	40.3	3.6	1.5
$Ce_3Fe_{25.0}Cr_{4.0}H_{5.4}$	398	38.6	34.0	1.2	0.7
$Nd_3Fe_{24.5}Cr_{4.5}H_{5.0}$	488	37.9	40.8	4.0	1.6
$Sm_3Fe_{24.0}Cr_{5.0}H_{4.2}$	474	37.6	32.7	10.3	2.9
$Gd_3Fe_{28.0}Cr_{1.0}H_{4.2}$	571	37.6	42.1	8.4	2.9
$Tb_3Fe_{28.0}Cr_{1.0}H_{4.2}$	554	25.0	34.9	9.6	1.5
$Tb_3Fe_{27.0}Cr_{2.0}H_{2.8}$	530	22.6	33.0	10.6	4.3
$Dy_3Fe_{27.4}Cr_{1.6}H_{2.1}$	508	21.9	32.5	11.6	2.7

But the variations of the anisotropy field both at 4.2 K and RT upon hydrogenation for $R_3Fe_{29-x}Cr_x$ with R = Ce, Nd, Gd, and Tb ($x = 1.0$) display a complicated behaviour, due to the varying Cr concentration (x) and the varying H concentration (y).

The saturation magnetization of $Y_3Fe_{27.2}Cr_{1.8}H_{3.8}$ at 4.2 K is 43.0 μ_B/f.u. corresponding to an average Fe magnetic moment of 1.58 μ_B/Fe. Hydrogenation leads to a decrease of 0.34 μ_B/Fe in the average Fe magnetic moment compared with that in $Y_3Fe_{27.2}Cr_{1.8}$ at 4.2 K. After hydrogenation, the decrease or increase in the saturation magnetization for other hydrides is determined by the net magnetic moment of the R and Fe sublattices owing to the ferromagnetic or antiferromagnetic coupling between the magnetic moments of the R and Fe sublattices. A small increase in the anisotropy field of $Y_3Fe_{27.2}Cr_{1.8}H_{3.8}$ at 4.2 K is observed, which indicates that hydrogenation can slightly improve the planar magnetic anisotropy for the Fe sublattice in the $Y_3Fe_{27.2}Cr_{1.8}$ compounds at 4.2 K.

4. Conclusions

A systematic investigation of phase formation, crystallographic properties, and intrinsic magnetic properties of the hydrides $R_3Fe_{29-x}Cr_xH_y$ (R = Y, Ce, Nd, Sm, Gd, Tb, and Dy) has been performed in this work. Hydrogenation leads to a relative volume expansion of the unit cell of between 0.84% and 2.6%, and a corresponding decrease in x-ray density for each compound. The lattice constants and the unit-cell volume V of $R_3Fe_{29-x}Cr_x$ and $R_3Fe_{29-x}Cr_xH_y$ decrease with increasing R atomic number from Nd to Dy, except for Ce, reflecting the lanthanide contraction. The abnormal crystallographic and magnetic properties of $Ce_3Fe_{25.0}Cr_{4.0}$ and $Ce_3Fe_{25.0}Cr_{4.0}H_{5.4}$ indicate that the Ce ion is non-triply ionized. Hydrogenation leads to anisotropic expansions mainly along the a- and b-axes rather than along the c-axis for each compound. This result indicates that the hydrogen atoms mainly occupy the 4i and 4f sites with the $A2/m$ space group which are located in the basal plane referred to the 1:5 cell.

Hydrogenation results in an increase in the Curie temperature for each compound, and this leads to an increase in the saturation magnetization at RT for $R_3Fe_{29-x}Cr_x$ with R = Y, Ce, Nd, Sm, Gd, Tb, and Dy. The average Fe atomic magnetic moment μ_{Fe} at 4.2 K in $Y_3Fe_{27.2}Cr_{1.8}H_{3.8}$ is 1.58 μ_B/Fe, which is 0.34 μ_B/Fe lower than that in the compound $Y_3Fe_{27.2}Cr_{1.8}$.

$Ce_3Fe_{25.0}Cr_{4.0}$ and $Nd_3Fe_{24.5}Cr_{4.5}$, showing the larger content of hydrogen with $y = 5.4$ and 5.0 in these compounds, may be interesting candidates for further investigation in order to develop new hydrogen storage media.

Acknowledgments

This project was supported by the State Committee of Science and Technology and the National Natural Science Foundation of China, and in part by the CNPq-Brazil, the Japanese Society for the Promotion of Science, and the National Key Laboratory of Theoretical Computational Chemistry, Jilin University.

References

[1] Collocott S J, Day R K, Dunlop J B and Davis R L 1992 *Proc. 7th Int. Symp. on Magnetic Anisotropy and Coercivity in Rare-earth–Transition Metal Alloys (Canberra, 1992)* ed Hi-Perm Laboratory, Research Centre for Advanced Mineral and Material Processing, University of Western Australia, p 437
[2] Shcherbakova Ye V, Ivanova G V, Yermolenko A S, Belozerov Ye V and Gaviko V S 1992 *J. Alloys Compounds* **182** 199
[3] Li H S, Cadogan J M, Davis R L, Margarian A and Dunlop J B 1994 *Solid State Commun.* **90** 487
[4] Kalogirou O, Psycharis V, Saettas L and Niarchos D N 1995 *J. Magn. Magn. Mater.* **146** 335
[5] Yelon W B and Hu Z 1996 *J. Appl. Phys.* **79** 1330
[6] Hu Z, Yelon W B, Kalogirou O and Psycharis V 1996 *J. Appl. Phys.* **80** 2955
[7] Yang F M, Nasunjilegal B, Wang J L, Zhu J J, Qin W D, Tang N, Zhao R W, Hu B P, Wang Y Z and Li H S 1995 *J. Phys.: Condens. Matter* **7** 1679
[8] Hu B P, Liu G C, Wang Y Z, Nasunjilegal B, Zhao R W, Yang F M, Li H S and Cadogan J M 1994 *J. Phys.: Condens. Matter* **6** L197
[9] Hu B P, Liu G C, Wang Y Z, Nasunjilegal B, Tang N, Yang F M, Li H S and Cadogan J M 1994 *J. Phys.: Condens. Matter* **6** L595
[10] Fuerst C D, Pinkerton F E and Herbst J F 1994 *J. Appl. Phys.* **76** 6144
[11] Ryan D H, Cadogan J M, Margarian A and Dunlop J B 1994 *J. Appl. Phys.* **76** 6150
[12] Margarian A, Dunlop J B, Day R K and Kalceff W 1994 *J. Appl. Phys.* **76** 6153
[13] Nasunjilegal B, Yang F M, Zhu J J, Pan H Y, Wang J L, Qin W D, Tang N, Hu B P, Wang Y Z, Li H S and Cadogan J M 1996 *Acta Phys. Sinica* **5** 544
[14] Morellon L, Algarabel P A, Ibarra M R, Kamarád J, Arnold Z, Pareti L, Albertini F and Paoluzi A 1994 *J. Magn. Magn. Mater.* **150** L285
[15] Ibarra M R, Morellon L, Blasco J, Pareti L, Algarabel P A, García J, Albertini F and Paoluzi A 1994 *J. Phys.: Condens. Matter* **6** L717
[16] Li H S, Courtois D, Cadogan J M, Xu J M and Dou S X 1994 *J. Phys.: Condens. Matter* **6** L771
[17] Yang F M, Han X F, de Boer F R and Li H S 1997 *J. Phys.: Condens. Matter* **9** 1339
[18] Shcherbakova Ye V, Ivanova G V, Bartashevich M I, Khrabrov V I and Belozerov Ye V 1996 *J. Alloys Compounds* **240** 101
[19] Koyama K, Fujii H and Suzuki S 1996 *J. Magn. Magn. Mater.* **161** 118
[20] Han X F, Yang F M, Pan H G, Wang Y G, Wang J L, Liu H L, Tang N, Zhao R W and Li H S 1997 *J. Appl. Phys.* **81** 7450
[21] Han X F, Yang F M, Zhu J J, Pan H G, Wang Y G, Wang J L, Tang N and Zhao R W 1997 *J. Appl. Phys.* **81** 3248
[22] Courtois D, Li H S and Cadogan J M 1997 *IEEE Trans. Magn.* **33** 3844
[23] Kalogirou O, Psycharis V, Gjoka M, Niarchos D and Fuerst C D 1996 *J. Appl. Phys.* **79** 5539
[24] Suzuki S, Suzuki S and Awasaki M K 1995 *IEEE Trans. Magn.* **31** 3695
[25] Han X F, Pan H G, Liu H L, Yang F M and Zheng Y W 1997 *Phys. Rev.* B **56** 8867

[26] Fuerst C D, Pinkerton F E and Herbst J F 1994 *J. Magn. Magn. Mater.* **129** L115
[27] Pan H G, Yang F M, Chen Y, Han X F, Tang N, Chen C P and Wang Q D 1997 *J. Phys.: Condens. Matter* **9** 2499
[28] Nagamine L C C M, Souza Azevedo I, Baggio-Saitovitch E, Rechenberg H R, Han X F and Lin L Y 1998 *4th Latin-American Workshop on Magnetism, Magnetic Materials, and their Applications (São Paulo, Brazil); Adv. Mater. Res.* at press
[29] Müller K H, Dunlop J B, Handstein A, Gebel B and Wendhausen P A P 1996 *J. Magn. Magn. Mater.* **157+158** 117
[30] Han X F, Yang F M, Li Q S, Zhang M C and Zhou S Z 1998 *J. Phys.: Condens. Matter* **10** 151
[31] Han X F, Yang F M, Pan H G, Wang Y G and Wang Y Z 1998 *J. Appl. Phys.* **83** 4366
[32] Wang Y Z, Hu B P, Liu G C, Li H S, Han X F and Yang C P 1997 *J. Phys.: Condens. Matter* **9** 2787
[33] Wang Y Z, Hu B P, Liu G C, Li H S, Han X F and Yang C P 1997 *J. Phys.: Condens. Matter* **9** 2793
[34] Wiesinger G and Hilscher G 1991 *Handbook of Magnetic Materials* vol 6, ed K H J Buschow (Amsterdam: Elsevier) p 514
[35] Asti G and Bolzoni F 1985 *J. Appl. Phys.* **58** 1924